

Energetics of kinetic reconnection in a three-dimensional null points cluster

V. Olshevsky,^{1,2,*} G. Lapenta,¹ and S. Markidis³

¹*Center for mathematical Plasma Astrophysics (CmPA) Department of Mathematics, KU Leuven, Celestijnenlaan 200B, bus 2400 B-3001 Leuven, Belgium.*

²*Main Astronomical Observatory of NAS, Akademika Zabolotnoho 27, 03680, Kyiv, Ukraine*

³*High Performance Computing and Visualization (HPCViz), KTH Royal Institute of Technology, SE-100 44, Stockholm, Sweden*

We performed three-dimensional Particle-in-Cell simulations of magnetic reconnection with multiple magnetic null points. Magnetic field energy conversion into kinetic energy was about five times higher than in traditional Harris sheet configuration. More than 85% of initial magnetic field energy was transferred to particle energy during 25 reversed ion gyrofrequencies. Magnetic reconnection in the cluster of null points evolved in three phases. During the first phase, ion beams were excited, that then gave part of their energy back to magnetic field in the second phase. In the third phase, magnetic reconnection occurs in many small patches around the current channels formed along the stripes of low magnetic field. Magnetic reconnection in null points presents essentially three-dimensional features, with no two dimensional symmetries or current sheets.

Null-point magnetic reconnection is thought to be the main source of energy release in solar flares, Earth magnetosphere and other astrophysical plasmas. Simulations of 3D null point reconnection in magnetohydrodynamic (MHD) approach were reported in [1–3]; null-point reconnection regimes were reviewed and classified by [4]; in the papers [5, 6] 3D null point reconnection was studied in kinematic approach; [7–9] investigated particle acceleration in the vicinity of 3D null-points. In many astrophysical applications, such as planet magnetospheres or solar flares, fluid models are not sufficient to describe magnetic reconnection [10, 11]. To our knowledge, only [12] reported Particle-in-Cell (PIC) simulations of an isolated null point in solar corona. To understand the basic kinetic and 3D effects of null point reconnection, we have performed PIC simulation of a cluster of null points in the simplest possible configuration that excludes the complications due to boundary condition or external sources. We have found that energy release in such system is much more efficient than in traditional Harris sheet configurations. Three-dimensional effects dominate in the dynamics throughout the simulation, and no current sheets or other 2D structures are formed during reconnection. We believe that both laminar and turbulent reconnection regimes were realised in our experiment, characterized by different energy dissipation and particle acceleration [13–15].

Making the very first step towards kinetic models of 3D null point reconnection, we designed our simulations to be as simple and straightforward, as possible. In particular, we impose boundaries in our simulation domain periodic in all directions. In a fully periodic box, it can be proved that the minimum number of points where magnetic field vanishes, is 8. We have chosen a non-equilibrium initial state with uniformly spaced 8 null points:

$$B_x = -B_0 \cos\left(\frac{2\pi x}{L_x}\right) \sin\left(\frac{2\pi y}{L_y}\right),$$

$$B_y = B_0 \cos\left(\frac{2\pi y}{L_y}\right) \left(\sin\left(\frac{2\pi x}{L_x}\right) - 2 \sin\left(\frac{2\pi z}{L_z}\right) \right),$$

$$B_z = 2B_0 \sin\left(\frac{2\pi y}{L_y}\right) \cos\left(\frac{2\pi z}{L_z}\right),$$

where B_0 is the magnetic field amplitude; L_x , L_y , and L_z are the sizes of the simulation domain in the corresponding directions. It is easy to show that this configuration satisfies the condition $\nabla \cdot \mathbf{B} = 0$. Besides 8 null points, the condition $B = 0$ also holds along 9 “null lines” lied up in the planes $Y = \pi n$, where n is an integer (Fig. 1).

The collisionless plasma simulations were carried out using iPIC3D, fully kinetic electromagnetic PIC code with implicit time stepping [16]. Simulation domain represents a cubic box with dimensions $L_x \times L_y \times L_z = 10 d_i \times 10 d_i \times 10 d_i$ with 256^3 cells and 64 particles of each specie per cell. Our plasma consisted of electrons and ions with mass ratio $m_i/m_e = 25$ and temperature ratio $T_i/T_e = 5$; the particles were initialized with Maxwellian velocity distribution with electron thermal velocity $v_{the}/c = 0.0346$. The initial particle density was uniform with $n_0 = 1$; the initial magnetic field amplitude was $B_0 = 0.03$. It is important to note, that with such parameters the electron spatial scales are well resolved in our simulation: the electron skin depth $d_e = 0.2 d_i = 5\Delta x$, where Δx is the grid spacing. The time step was set relative to ion plasma frequency: $\Delta t = 0.125/\omega_{pi}$. For consistency, in the following all times are normalized to ion gyrofrequency computed with the initial field amplitude $\Omega_{ci} = eB_0/m_i c = 0.052 \omega_{pi}$.

Our simulation domain initially includes null points of both A and B types [17], as shown in Figure 1. All the null points are interconnected with each other by separators, formed by the intersections of separatrix surfaces and spines. Many of these separators are the artifacts of the highly symmetric configuration, and must not necessarily exist in nature [18]; they are destroyed very quickly after beginning of the simulation.

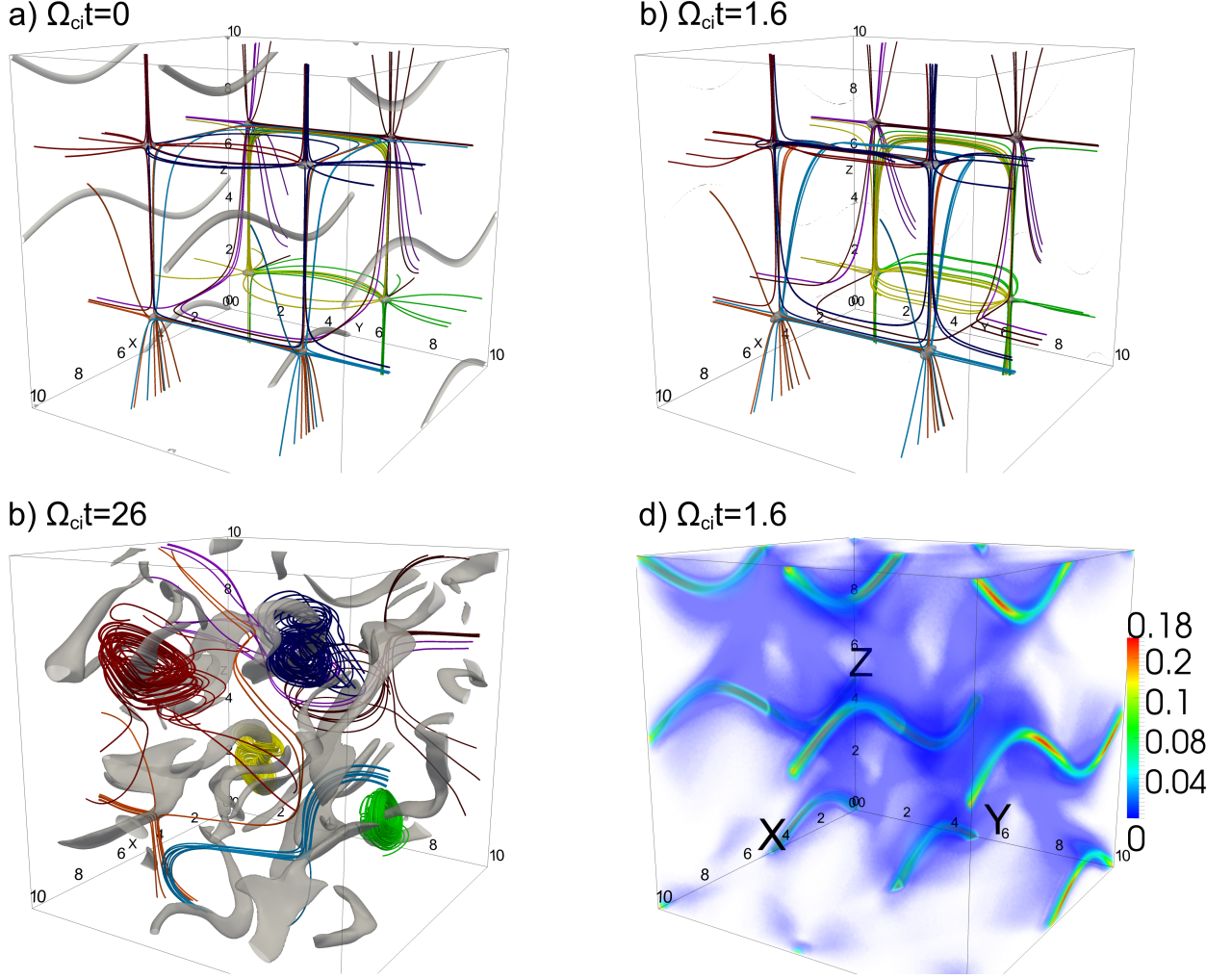


FIG. 1. **a, b, c:** Snapshots of magnetic field at different times (labelled in the upper left). Field lines are plotted in different colors; each color corresponds to the lines passing by one of 8 initial null points. Isocontours of low magnetic field $B = 0.1B_0$ are plotted in grey. **d:** Snapshot of current J made at $\Omega_{ci}t = 1.6$.

At $\Omega_{ci}t = 1.6$ (panel b in Fig. 1) no aforementioned “null line” is visible, and the connectivity of many field lines has changed. Initially, gas and magnetic pressures are not balanced, and the magnetic fields surrounding the “null lines” are compressed by plasma. Particles move towards these regions and establish the current channels that dominate the evolution of the system, as shown in panel d of Figure 1. The energy released by magnetic field in this phase of the simulation is transferred mainly to ions accelerated in the current channels. The radius of the cross-section of such channel is of the order of d_i . Current channels become unstable later in time, they are continuously distorted, and multiple stripes of small B intensity are formed along them. As we will demonstrate below, the reconnection sites are associated with these regions. There is no initial current through the null points in our configuration, and the null points do not move during the simulation. They are destroyed in pairs (see

article supplemented material).

At the end of the simulations all 8 null points are destroyed, and the magnetic field organization is not reminiscent of the initial configuration. The magnetic field lines spiral around current channels established in the regions of low B . Note, that we have terminated the simulation at time $\Omega_{ci}t = 26$ when most, but not all the magnetic field lines are reconnected. All the features forming during the simulation are essentially three-dimensional, and current sheets or other 2D structures are not created.

Figure 2 shows the evolution of the magnetic field energy W_{mag} , total kinetic energy of the particles W_{kin} , bulk and thermal kinetic energy for species ($W_{bulk,e}$, $W_{bulk,i}$, $W_{therm,e}$, and $W_{therm,i}$, correspondingly). The electric field energy is two orders of magnitude smaller than other components of energy, and is not shown in the plot. Initially, the magnetic energy contributes 85% to the total energy of the system; particles contribute only

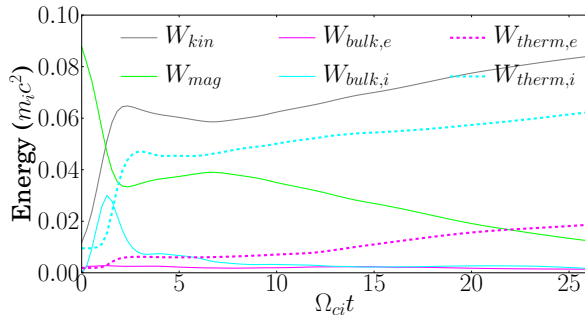


FIG. 2. Evolution of different components of energy (total kinetic energy of particles, magnetic field energy, bulk and thermal energy of both species).

12%. At the end of the simulation, particle energy constitutes 87% of the total energy: 86% of magnetic energy is released within $26\Omega_{ci}^{-1}$. This corresponds to decay rate $\lambda = (\Delta W_{mag}/\Delta t)/W_{mag} \approx 0.033\Omega_{ci}$, which is almost 5 times higher than $\lambda \approx 0.0075\Omega_{ci}$ observed in “classical” two-dimensional Harris current sheet reconnection setup [19, 20].

In the beginning of the simulation, when the current channels are established, most of the released magnetic energy goes to the energy of ion bulk motions $W_{bulk,i}$. Very soon, though, these motions are slowed down, and in the later phase of reconnection the temperature of species is increased rather than fluid motions. At the end of the simulations temperature ratio reduces to $T_i/T_e \approx 3$, and fluid motions constitute only a few percent to the total energy in the system.

As in [21, 22], we compute the electron-frame dissipation measure

$$D_e = \mathbf{J} \cdot (\mathbf{E} - [\mathbf{J}_e \times \mathbf{B}]/\rho_e) + \rho_c \mathbf{u}_e \cdot \mathbf{E}, \quad (1)$$

where \mathbf{J} and \mathbf{J}_e are the total and electron current densities, correspondingly, ρ_e and \mathbf{u}_e are electron density and speed, and $\rho_c = e(n_i - n_e)$ is charge density. The dissipation D_e characterizes the work done by fields on particles $\mathbf{J} \cdot \mathbf{E}$ with corrections for convective motions $\mathbf{J} \cdot [\mathbf{J}_e \times \mathbf{B}]/\rho_e$, and for charge separation $\rho_c \mathbf{u}_e \cdot \mathbf{E}$. The latter quantity is by orders of magnitude smaller than two other components of D_e in our simulations. The first two components balance each other so that D_e is very small.

For additional illustration, we have selected the “lower” half of our computational domain that spans from $Z = 0$ to $Z = 5d_i$, and contains 4 null points and sections of 6 “null lines”. Figure 3 shows snapshots of D_e and parallel electric field $E_{\parallel} = \mathbf{E} \cdot \mathbf{B}/B$ in this slab.

The magnetic reconnection dynamics may be divided into three distinct phases according to the energy evolution. The first phase of rapid acceleration of particles and very high dissipation D_e lasts till $\Omega_{ci}t \approx 2$. During this time powerful currents are established in the low B value channels. The speeds of particle beams in these channels

are up to $3.3V_A$ for electrons and $1.6V_A$ for ions, where V_A is Alfvén speed. Most of the electromagnetic energy at this stage goes to accelerate ion fluid motions; electron acceleration is much smaller. The dissipation regions and the regions of enhanced E_{\parallel} surround the current channels (left column in Fig. 3).

During the second phase of magnetic reconnection, $2.5 \lesssim \Omega_{ci}t \lesssim 7$, work of the electromagnetic field on particles is negative, i.e., particles give some of their energy back to the field. The main contributor of this “reverse” energy exchange is the deceleration of ion currents. Dissipation areas surround the current channels, while the regions of large values of E_{\parallel} are scattered randomly throughout the domain, so there is no correlation between these locations (middle column in Fig. 3). The value of $T_i/T_e \approx 3$ establishes in this phase, and does not substantially vary later.

In the last phase of magnetic reconnection, small-scale reconnection events are chaotically distributed in the regions of low B (right column in Fig. 3). The locations of enhanced D_e and E_{\parallel} show well correspondence to each other. This phase is characterized by a steady growth of particle energy and a decrease of the magnetic energy (Fig. 2). The released magnetic energy accelerates particle random motions and increase their effective temperature. The steady (turbulent) reconnection process continues until all the null points are destroyed and all field lines reconnect (not shown in this paper).

To summarize, we have performed PIC simulations of magnetic reconnection in a 3D domain that contains 8 null points. The simulation was terminated at $\Omega_{ci}t = 26$, when all the initial null points vanish, and the majority of magnetic field lines spiral around the regions of low magnetic field and powerful electric currents. During this period, 86% of initial magnetic field energy was transferred to particle kinetic energy, and the decay rate was almost 5 times higher than in two-dimensional Harris sheet reconnection. All the magnetic and current features that formed during the simulations were essentially three-dimensional, no current sheets or other 2D structures were identified.

Three phases of magnetic reconnection could be distinguished: (i) a rapid establishment of powerful current channels, when most of energy is gained by ion beams; (ii) a negative dissipation phase, when ion beams slow down and return some energy back to electromagnetic field; (iii) a “steady” reconnection phase, characterized by multiple small-scale reconnection events localized around the current channels. The first two phases lasted for $\Omega_{ci}t \approx 2$, and $\Omega_{ci}t \approx 5$, correspondingly, while the third one was still developing when the simulation was terminated. Finally, most of the magnetic energy was converted to the thermal energy of the particles, so that ion/electron temperature ratio changed from 5 in the beginning to 3 in the end of simulations.

Interestingly, during the second phase the topology of

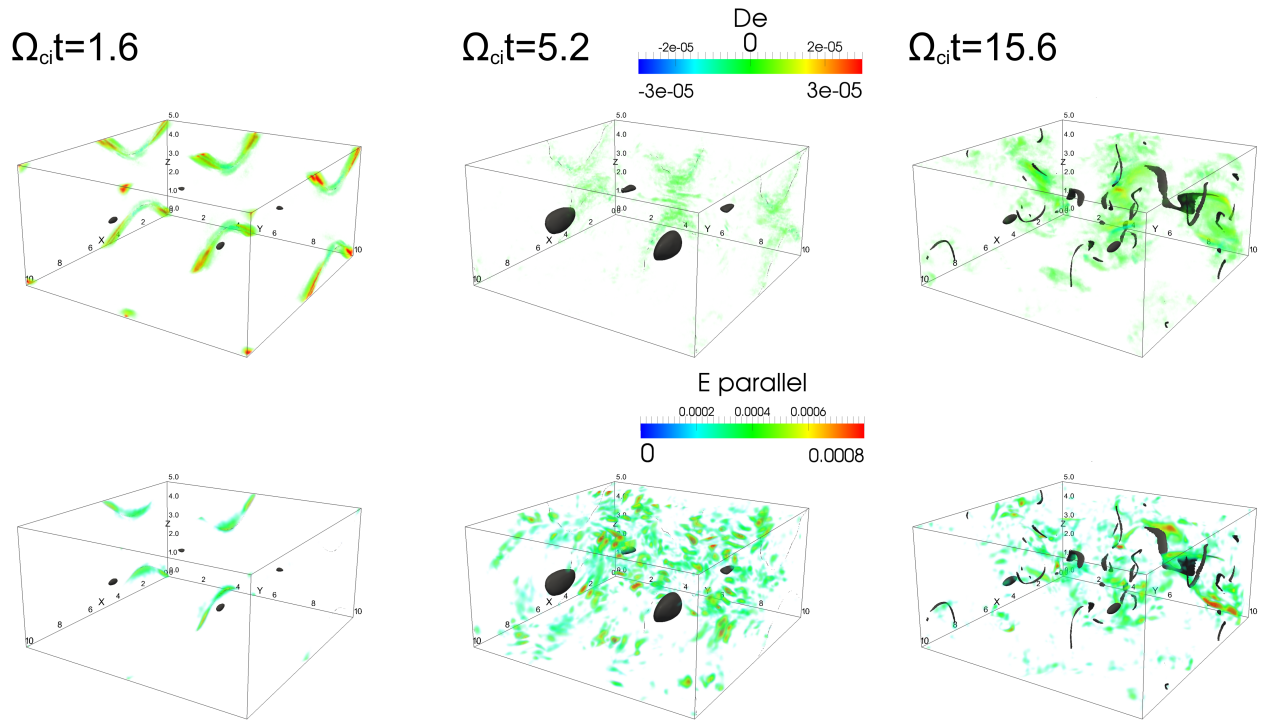


FIG. 3. Snapshots of the electron-frame dissipation measure D_e (upper panels) and parallel electric field E_{\parallel} (lower panels) in the lower half of the computational domain spanning from $Z = 0$ to $Z = 5d_i$ at different times (labelled in the upper left of each column). Isocontours of low magnetic field $B = 0.1B_0$ are plotted in grey.

magnetic field was changing, but the dissipation regions did not coincide with the regions of enhanced parallel electric field. During the “steady” reconnection, however, these locations showed good correspondence to each other, surrounding the regions where the reconnection took place.

Authors are grateful to Dr. Clare Parnell for the useful comments on the structure of the magnetic configuration. This research has received funding from the European Commission’s FP7 Program with the grant agreement SWIFF (project 2633430, swiff.eu). The simulations were conducted on the computational resources provided by the PRACE Tier-0 project 2011050747 (Curie supercomputer)

* vyacheslav.olshevsky@wis.kuleuven.be

- [1] K. Galsgaard and Å. Nordlund, *J. Geophys. Res.* **102**, 231 (1997).
- [2] K. Galsgaard and D. I. Pontin, *Astron. Astrophys.* **529**, A20 (2011).
- [3] K. Galsgaard and D. I. Pontin, *Astron. Astrophys.* **534**, A2 (2011).
- [4] E. R. Priest and D. I. Pontin, *Phys. Plasmas* **16**, 122101 (2009).
- [5] Y.-T. Lau and J. M. Finn, *Astrophys. J.* **350**, 672 (1990).
- [6] D. I. Pontin, G. Hornig, and E. R. Priest, *Geophysical*

- and *Astrophysical Fluid Dynamics* **99**, 77 (2005).
- [7] S. Dalla and P. K. Browning, *Astron. Astrophys.* **436**, 1103 (2005).
- [8] J.-N. Guo, J. Büchner, A. Otto, J. Santos, E. Marsch, and W.-Q. Gan, *Astron. Astrophys.* **513**, A73 (2010).
- [9] A. Stanier, P. Browning, and S. Dalla, *Astron. Astrophys.* **542**, A47 (2012).
- [10] H. Ji and W. Daughton, *Phys. Plasmas* **18**, 111207 (2011).
- [11] S. D. Baalrud, A. Bhattacharjee, Y.-M. Huang, and K. Germaschewski, *Phys. Plasmas* **18**, 092108 (2011).
- [12] G. Baumann and Å. Nordlund, *Astrophys. J. Letts.* **759**, L9 (2012).
- [13] D. Biskamp, *Physics of Fluids* **29**, 1520 (1986).
- [14] A. Lazarian and E. T. Vishniac, *Astrophys. J.* **517**, 700 (1999).
- [15] G. Lapenta, *Phys. Rev. Lett.* **100**, 235001 (2008).
- [16] S. Markidis, G. Lapenta, and Rizwan-uddin, *Mathematics and Computers and Simulation* **80**, 1509 (2010).
- [17] S. W. H. Cowley, *Radio Science* **8**, 903 (1973).
- [18] J. M. Greene, *J. Geophys. Res.* **93**, 8583 (1988).
- [19] S. Markidis, G. Lapenta, A. Divin, M. Goldman, D. Newman, and L. Andersson, *Phys. Plasmas* **19**, 032119 (2012).
- [20] A. E. Vapirev, G. Lapenta, A. Divin, S. Markidis, P. Henri, M. Goldman, and D. Newman, *J. Geophys. Res.: Space Physics*, n/a (2013).
- [21] M. Wan, W. H. Matthaeus, H. Karimabadi, V. Roytershteyn, M. Shay, P. Wu, W. Daughton, B. Loring, and S. C. Chapman, *Phys. Rev. Lett.* **109**, 195001 (2012).
- [22] S. Zenitani, M. Hesse, A. Klimas, and M. Kuznetsova, *Phys. Rev. Lett.* **106**, 195003 (2011).